NO-binding in Ru(NO) 2 8 -type [Ru(NO) 2 (PR 3) 2 X]BF 4 compounds

Anna Gallien, Dominik Schaniel, Theo Woike, Peter Klüfers

Dalton Transactions

PAPER

View Article Online
View Journal | View Issue

Cite this: *Dalton Trans.*, 2014, **43**, 13278

NO-binding in $\{Ru(NO)_2\}^8$-type $[Ru(NO)_2(PR_3)_2X]BF_4$ compounds†

Anna K. E. Gallien,[a] Dominik Schaniel,*[b,c] Theo Woike[d] and Peter Klüfers*[a]

Two different structure types were found for a series of mononuclear dinitrosyl complexes of the general formula $[RuL_2(NO)_2X]BF_4$ (L = monodentate phosphane, X = Cl, Br, I). The $\{Ru(NO)_2\}^8$-type target compounds were prepared by the reduction of the respective $\{RuNO\}^6$ precursors and subsequent oxidative addition of $(NO)BF_4$. About one half of the new compounds share their molecular structure with the hitherto only representative of this class of dinitrosyls, Pierpont and Eisenberg's $[RuCl(NO)_2(PPh_3)_2]PF_6{\cdot}C_6H_6$ (*Inorg. Chem.*, 1972, **11**, 1088–1094). The C_s-symmetric cations exhibit both a linear and a bent Ru–N–O fragment, in line with a formal 6 + 2 split of the $\{Ru(NO)_2\}^8$ electron sum in the sense of a $[Ru^{II}(NO^+)(^1NO^-)]^{2+}$ bonding. The coordination entity's configuration in this subgroup is described by IUPAC's polyhedral symbol *SPY*-5. Continuous shape measures (CShM) as defined by Alvarez *et al.* (*Coord. Chem. Rev.*, 2005, **249**, 1693–1708) reveal a uniform deviation from the L–M–L angles expected for *SPY*-5, in a narrower sense, towards a vacant octahedron (*vOC*-5). DFT calculations confirmed that Enemark and Feltham's analysis (*Coord. Chem. Rev.*, 1974, **13**, 339–406) of the electronic situation of the $\{Ru(NO)_2\}^8$ group remains adequate. The same holds for the second subclass of new compounds the existence of which had been predicted in the same paper by Enemark and Feltham, namely C_{2v}-symmetric, *TBPY*-5-type cations with two almost equally bonded nitrosyl ligands. In agreement with an 8 + 0 distribution of the relevant electrons, the formal $[Ru^0(NO^+)_2]^{2+}$ entities are found for L/X couples that donate more electron density on the central metal. Two solid compounds (**8a**/**b**, **12a**/**b**) were found in both structures including the special case of the P^iPr_3/Br couple **12a**/**b**, which led to crystals that contained both structure types in the same solid. Conversely, four compounds showed a single form in the solid but both forms in dichloromethane solution in terms of the solutions' IR spectra. The irradiation of crystalline **12** with blue laser light resulted in the photoisomerisation of, mainly, the bent $^1NO^-$ ligand in terms of low-temperature IR spectroscopy.

Received 22nd May 2014,
Accepted 13th July 2014

DOI: 10.1039/c4dt01506a

www.rsc.org/dalton

Introduction

As nitrogen monoxide is a "non-innocent", that is, redoxactive, potentially ambident ligand produced endogenously from L-arginine *via* nitric-oxide-synthase (NOS) catalysis in physiological signal transduction pathways, this simple molecule is one of the most interesting and challenging ligands in bioinorganic and coordination chemistry.[1]

The redox activity is due to the radical character of nitrogen monoxide which enables its participation in metal complexes in four different binding modes exhibiting different M–N–O angles: strongly bent (*ca.* 120°) as $^1NO^-$ in a low-spin complex, weakly bent (*ca.* 140°) as a neutral $^2NO^{\bullet}$ radical in a low-spin complex, (almost) linear as either a $^3NO^-$ diradical in a high-spin complex or a formal $^1NO^+$, the "formal" emphasising the high π acidity of the $^1NO^+$ ligand which hardly is a cation due to extensive back-bonding.

The analysis of the electronic structure of an M–N–O moiety is usually based on the spectroscopic and X-ray-crystallographic data of the compound in question. In order to enable a classification of nitrosyl complexes independent of their actual bonding modes, the Enemark–Feltham notation was

[a]*Fakultät für Chemie und Pharmazie, Butenandtstraße 5-13, 81377 Munich, Germany. E-mail: kluef@cup.uni-muenchen.de; Fax: +49 (0)89 2180 77407; Tel: +49 (0)89 2180 77404*
[b]*Université de Lorraine, CRM2, UMR 7036, Vandoeuvre les Nancy, F-54506, France. E-mail: dominik.schaniel@univ-lorraine.fr; Fax: +33 (0)383 68 43 00; Tel: +33 (0)3 83 68 48 70*
[c]*CNRS, CRM2, UMR 7036, Vandoeuvre les Nancy, F-54506, France*
[d]*TU Dresden, Institut für Strukturphysik, Zellescher Weg 16, 01069 Dresden, Germany. E-mail: theo.woike@tu-dresden.de; Fax: +49 (0)351 463 37048; Tel: +49 (0)351 463 32536*

†Electronic supplementary information (ESI) available: Details of crystallographic studies. CCDC 985278–985281, 985283–985289, 986283–986284. For ESI and crystallographic data in CIF or other electronic format see DOI: 10.1039/c4dt01506a

introduced, wherein the sum of the metal d electrons and the electrons in the π*(NO) orbital(s) is noted.[2] In this context, the dinitrosyl compounds of this work are of the $\{Ru(NO)_2\}^8$ type.

In the electronic and structural ground state (GS), the NO ligand of related NO^+-type mononitrosyl complexes is κ*N*-bonded. Upon irradiation with light, the metal–nitrosyl bond may be cleaved, resulting in the common photochemical property of NO release, which is used in PDT (photodynamic therapy) to liberate NO in a controlled manner at the target tissue.[3,4] As a more intricate type of excitation decay, the potentially ambident NO ligand may be switched into metastable bonding modes instead of dissociating from the metal centre. As a result, two such metastable modes have been detected in solid samples: the κ*O*-bonded, isonitrosyl, MS1 state and the κ^2*N*,*O*-bonded, side-on, MS2 state (Fig. 1 shows these modes for $\{RuNO\}^6$ centres).[5–7]

This phenomenon is referred to as photoinduced linkage isomerism (PLI). Since the excited states are long-lived below their specific temperature of decay, they can be detected and analysed *via* low-temperature IR spectroscopy, photocrystallography and DSC (differential scanning calorimetry). PLI has been well studied for $\{RuNO\}^6$ compounds, in which a single NO^+-type ligand is attached linearly to the metal centre. A $^1NO^-$-type nitrosyl has been described as photo-excitable as well, but, until now, for a $\{PtNO\}^8$ mononitrosyl complex only.[8,9] So far, photoinduced phenomena have not been investigated for $\{Ru(NO)_2\}^8$ dinitrosyl compounds.[5,10–12] Moreover, ruthenium–dinitrosyl chemistry appears largely underdeveloped in general, particularly in contrast to the chemistry of the homologous dinitrosyl iron compounds (DNICs) which are mostly of the $\{Fe(NO)_2\}^9$ and $\{Fe(NO)_2\}^{10}$ type.[13] (For DNICs, the PLI issue has been addressed as well.[14]) The mere number of only six published $\{Ru(NO)_2\}^n$-type compounds, four of which are of the $\{Ru(NO)_2\}^8$ type (**A–D** in Fig. 2), underlines this statement. In terms of structural and spectroscopic parameters, the electronic state of these $Ru(NO)_2$ moieties is characterised by one NO^+ and one $^1NO^-$ ligand (Fig. 2).

The issue of $NO^+/^1NO^-$ equilibration in **A** has attracted considerable interest in the past. On the one hand, in crystals of **A**, an easily distinguishable $NO^+/^1NO^-$ couple in a square pyramidal complex cation prevails. On the other hand, a dynamic interconversion of the nitrosyl bonding modes within the $Ru(NO)_2$ moiety was detected by ^{15}N NMR spectroscopy. Moreover, the symmetrised intermediate was not a transition state but a well populated intermediate in solution.[15] A prototype for the trigonal bipyramidal structure of the intermediate was provided by a related osmium homologue that showed this structure in the solid.[16]

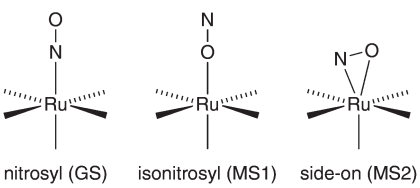

Fig. 1 Schematic illustration of the GS, MS1 and MS2 bonding mode in octahedral $\{RuNO\}^6$ complexes.

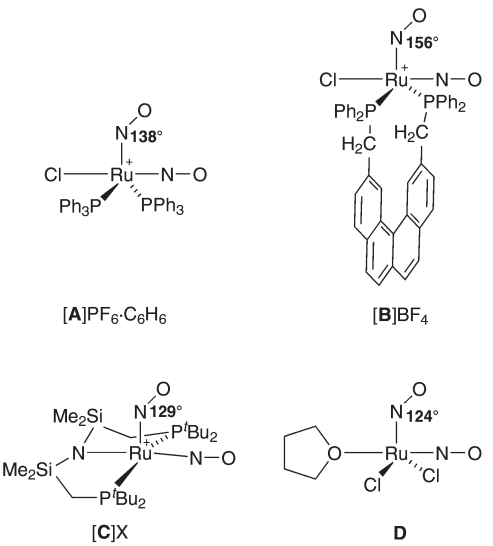

Fig. 2 Known $\{Ru(NO)_2\}^8$ dinitrosyls (charges are drawn at the central metal atom); several publications deal with salts of **A**, including a tetrafluoridoborate with a $^{14}NO/^{15}NO$ couple.[15,17–19] The "X" in [**C**]X is $[Ru(NO)(OH)(NO_2)_2Cl_2]$.[20–22] Ru–N–O angles are given for the bent RuNO moiety.

In this work, we extend the class of halogenido-bis(phosphane)-type $\{Ru(NO)_2\}^8$ compounds by new members with the goal of investigating the photoexcitability of dinitrosyl complexes. Specifically, we address some open questions of nitrosyl bonding and activation: (1) is the $NO^+/^1NO^-$ couple the usual bonding mode in $\{Ru(NO)_2\}^8$ dinitrosyls with the equilibrated form as a less stable intermediate? (2) Are $\{Ru(NO)_2\}^8$ dinitrosyls photoexcitable? (3) If so, which type of nitrosyl ligand, NO^+ or NO^-, is the switched one? To answer these questions, a series of bis-phosphane complex salts of the formula $[Ru(NO)_2(PR_3)_2X]BF_4$ (X = Cl, Br, I) is presented. This report focuses on the first of the three goals. The issues (2) and (3) are addressed for one of the new compounds to demonstrate the principal qualification of the new dinitrosyl complexes for photophysical research. Photoexcitation studies on other members will be published in a separate work in a more physical context.

Results and discussion

Synthesis

The synthesis of the target compounds followed the reaction scheme outlined in Fig. 3. The first step was the coordination of two equivalents of the respective phosphane (Fig. 3) to a $\{RuNO\}^6$ fragment in a *trans*-configuration. Depending on the phosphane, the reaction takes place either as a simple ligand substitution (route *i*) or as a redox reaction with the simultaneous addition of two equivalents of the respective phosphane (route *ii*). In the next step (*iii*), the respective $\{RuNO\}^n$

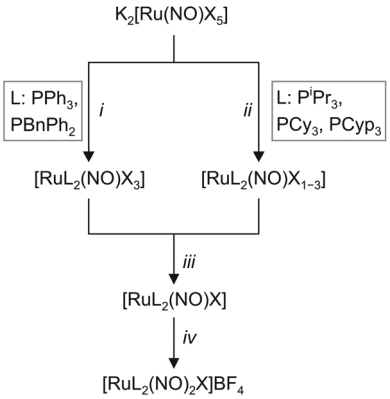

Fig. 3 Synthetic route to the $[RuL_2(NO)_2X]BF_4$ dinitrosyls of this work. The employed phosphanes differ by their electronic and steric properties as given by their Tolman's parameters (ν in cm^{-1} and cone angle): triphenylphosphane (PPh_3) 2068.9, 145°; benzyldiphenylphosphane ($PBnPh_2$) 2068.4, 152°, triisopropylphosphane (P^iPr_3) 2059.2, 160°; tricyclohexylphosphane (PCy_3) 2056.4, 170°; no values were available for tricyclopentylphosphane ($PCyp_3$). Details of the individual steps: *i* 2.5–3 eq. L, EtOH–H_2O; *ii* 2.5–4 eq. L, EtOH–H_2O; *iii* Zn_xCu, toluene; *iv* $(NO)BF_4$, toluene–EtOH. In the *ii* step, partial reduction of the Ru species by the more electron rich phosphanes took place prior to the final reduction step *iii*, hence the $[RuL_2(NO)X_{1-3}]$ formulation. Further details are collected in the Experimental section.

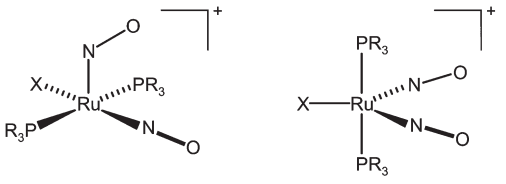

	PR_3/X
1	PPh_3/Cl
2	PPh_3/Br
5	PCy_3/Cl
6	PCy_3/Br
8a	$PCyp_3/Cl$
11	P^iPr_3/Cl
12a	P^iPr_3/Br

	PR_3/X
3	PPh_2Bn/Cl
4	PPh_2Bn/Br
7	PCy_3/I
8b	$PCyp_3/Cl$
9	$PCyp_3/Br$
10	$PCyp_3/I$
12b	P^iPr_3/Br

Fig. 4 The crystalline compounds of this work and their structure type. The abbreviations *TBPY*-5 and *vOC*-5 refer to IUPAC's configuration index and the definitions used by the Alvarez group in the context of *Continuous Shape Measures (CShM)*.[23]

(n = 6, 7, 8) fragment was treated with a zinc/copper alloy to ensure that all $\{RuNO\}^n$ mixtures were uniformly reduced to the $\{RuNO\}^8$ state. In the last step *iv*, the second nitrosyl ligand was introduced by the reaction of the $\{RuNO\}^8$ intermediate with $NOBF_4$ to form the attempted pentacoordinate dinitrosyl complex of the general formula $[RuX(NO)_2(PR_3)_2]BF_4$.

Crystalline products, including some as yet unknown iodido and bromido $\{Ru(NO)_2\}^8$ derivatives, were obtained by covering dichloromethane solutions with a layer of diethyl ether or *n*-pentane. The isolated crystals' colour depended on the halide, ranging from yellow to reddish brown.

Structural data

Crystal structure analyses revealed two structure types for the monocationic, pentacoordinate coordination entities: first, a vacant octahedron (*vOC*-5) with linear/bent Ru–N–O couples, and, second, a trigonal bipyramid (*TBPY*-5) with equilibrated Ru–N–O angles. An overview of the compounds, their numbering and the adopted structure type is given in Fig. 4.

To illustrate the structural principles, the cations in crystals of **1**, **3**, **8a**/**b**, **9**, **10**, and **12a**/**b** are depicted in Fig. 5–12. Significant bond distances and angles are collected in Table 1. Crystallographic data for all compounds as well as drawings and metrical parameters for **2**, **4**, **5**–**7** and **11** are collected in the ESI.†

The members of the first group resemble Pierpont and Eisenberg's prototypic dinitrosyl **A** (Fig. 2). They share the structural property of well separated bent/linear $^1NO^-/NO^+$ nitrosyl bonding.[17] In terms of the Enemark–Feltham notation, a ruthenium(II) centre contributes its six 4d electrons to

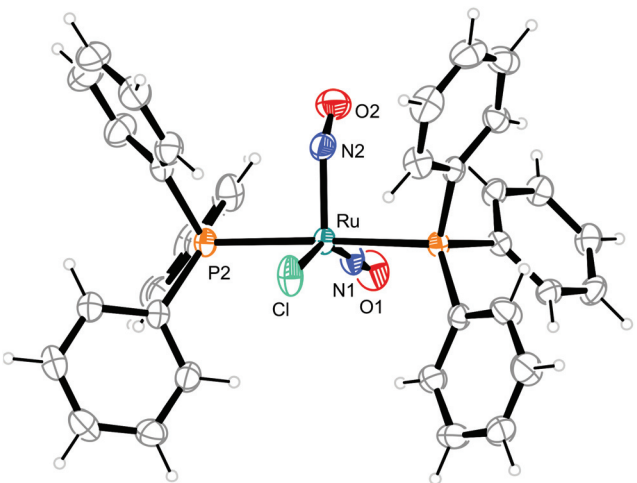

Fig. 5 Structure (50% ellipsoids) of the *vOC*-5-type complex cation in crystals of $[RuCl(NO)_2(PPh_3)_2]BF_4$ (**1**).

the $\{Ru(NO)_2\}^8$ formula, an NO^+ ligand none and a $^1NO^-$ ligand two electrons. This description also applies to **1**, **2**, **5**, **6**, **8a**, **11**, and **12a**. Geometrically, the structure type is characterised by a considerable difference of the two Ru–N–O angles (projection of the data points of Fig. 13 on the ordinate; note that a reliable separation of the two groups succeeds by the combination of ΔRuNO as a structural and $\Delta\nu$(NO) as a spectroscopic parameter [Fig. 13]). In terms of continuous shape measures (CShM), the complex cations are best described as vacant octahedra (*vOC*-5; in a vacant octahedron, the central atom is closer to the basal plane than it is in the *SPY*-5 conformation in the sense of ref. 23; the applicable IUPAC recommendation does not note this difference).[24] If Addison's τ_5 parameter was used to assign the conformation, the square pyramid resulted (sqp; using τ_5 categories, there is no differ-

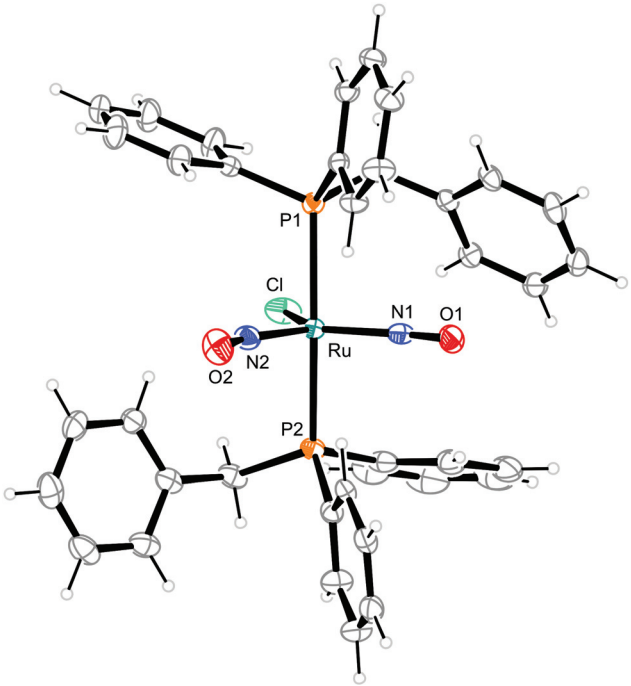

Fig. 6 Structure (50% ellipsoids) of the *TBPY*-5-type complex cation $[RuCl(NO)_2(PPh_2Bn)_2]^+$ in crystals of **3**.

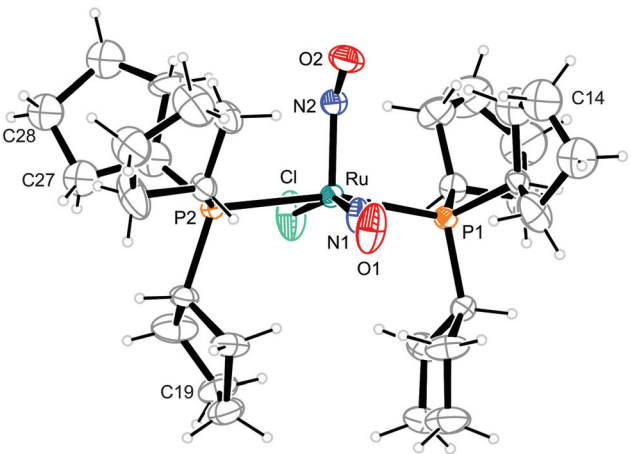

Fig. 7 Structure of the *vOC*-5-type complex cation $[RuCl(NO)_2(PCyp_3)_2]^+$ in crystals of **8a**. The thermal ellipsoids are drawn at 40% probability level. Some carbon atoms are disordered. The minor parts of C14 (44%), C19 (42%) and C27 and C28 (47%) are not shown. C13–15 and C26–29 were refined isotropically.

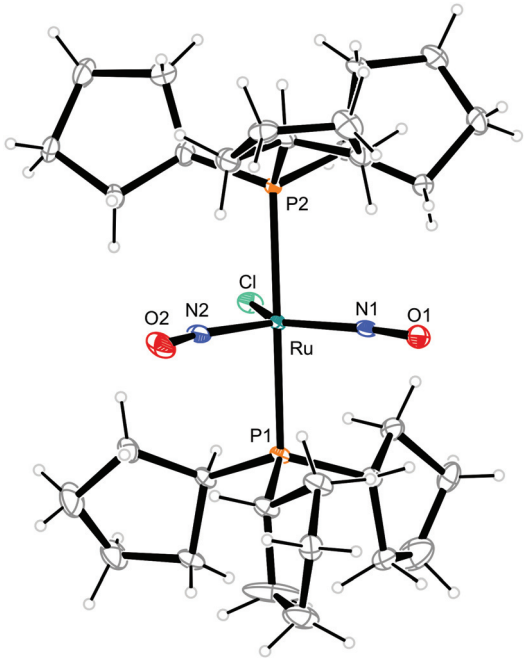

Fig. 8 Structure (50% ellipsoids) of the *TBPY*-5-type complex cation $[RuCl(NO)_2(PCyp_3)_2]^+$ in crystals of **8b**.

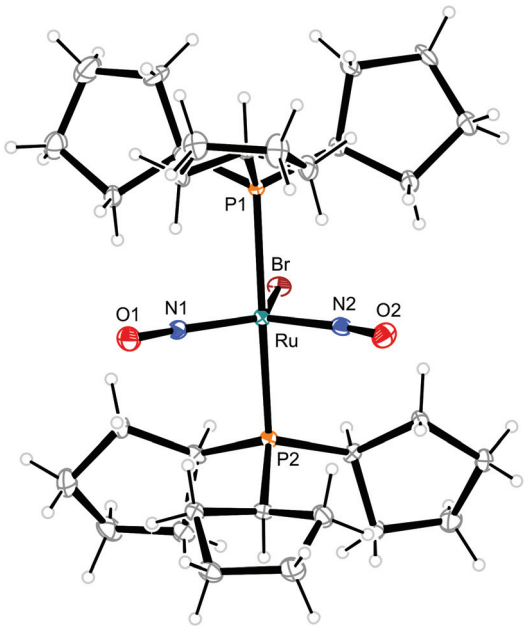

Fig. 9 Structure (50% ellipsoids) of the *TBPY*-5-type complex cation $[RuBr(NO)_2(PCyp_3)_2]^+$ in crystals of **9**.

ence between *vOC*-5 and *SPY*-5; hence, in this work, the CShM terminology is used).[25] The bent nitrosyl ligand forms the apex of the vacant octahedron and the *trans*-configured phosphanes together with the halide ligand and the linear NO group comprises the basal plane (Table 1). The mean P–Ru–P angle deviates from linearity by 14.5° since the phosphorus atoms are bent away from the bent NO group. The two NO ligands are clearly distinct from each other, not only in terms of the Ru–N–O-angle difference which ranges from 26.2° to 44.1°, but also in terms of the Ru–N bond length difference (0.090 to 0.140 Å, Table 1). The oxygen atom of the bent NO group points towards the linear nitrosyl ligand. The maximum symmetry for these compounds is that of point group C_s.

The members of the second, the *TBPY*-5 group, are well separated in terms of metrical parameters. Hence, the structure of the cations in **3**, **4**, **7**, **8b**, **9–10**, and **12b** resembles that of the

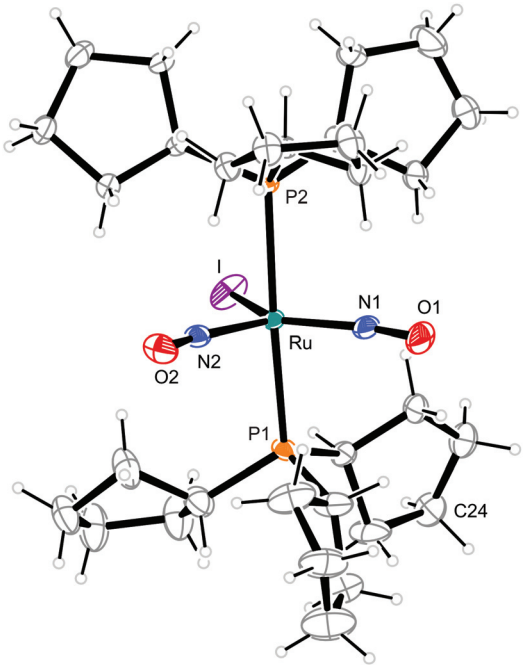

Fig. 10 Structure (50% ellipsoids) of the *TBPY*-5-type complex cation $[RuI(NO)_2(PCyp_3)_2]^+$ in crystals of **10**. C24 is disordered, the minor part (34%) is not shown.

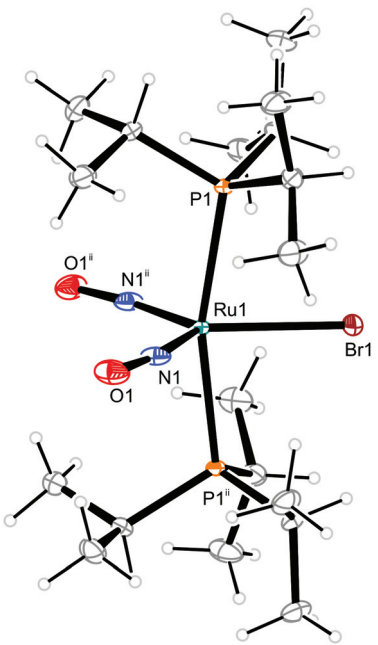

Fig. 11 Structure (50% ellipsoids) of the *TBPY*-5-type conformer **12b** of the complex cation $[RuBr(NO)_2(P^iPr_3)_2]^+$ in crystals of **12**. Symmetry code: [ii] $-x + 1, y, -z + 1/2$.

nitrosyl-equilibrated intermediate described in the introduction. The structure type is best described as a trigonal bipyramid (*TBPY*-5) in terms of CShM (and τ_5) values (CShM values are collected in the ESI†). The *trans*-arranged phosphane ligands form the apexes of the bipyramid, the halide together

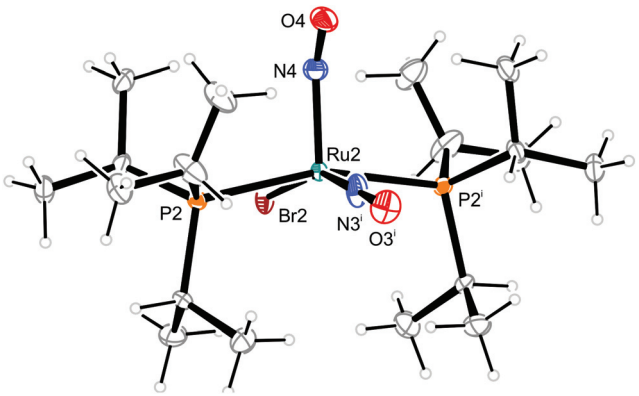

Fig. 12 Structure (50% ellipsoids) of the *vOC*-5-type conformer **12a** of the complex cation $[RuBr(NO)_2(P^iPr_3)_2]^+$ in crystals of **12**. Symmetry code: [i] $-x, y, -z + 1/2$. The linear NO group and the Br ligand are disordered in such a way as to be superimposed onto each other. The bent NO group is also disordered in such a way to ensure that the O4 atom is always inclined to the linear NO group. This kind of disorder corresponds to crystallographic *mm*2 site symmetry of the cations.

with the two NO groups form the trigonal plane. Again, the P–Ru–P angle deviates from linearity by 14.0° on average. The phosphorus atoms are bent away from the NO groups, the nitrosyl ligands themselves are slightly bent (13.5° in average) in a cisoid fashion. The equilibration of the two NO ligands is mirrored in the angles and the distances of the $Ru(NO)_2$ moieties, the Ru–N–O angle difference ranging from 0.0 to 7.2°, the Ru–N distances differing by 0.016 Å in maximum. The trigonal-bipyramidal conformation had been as yet unknown for pentacoordinate $\{Ru(NO)_2\}^8$ compounds with simple monodentate co-ligands. The maximum symmetry reachable in these structures refers to point group C_{2v}, which is the crystallographic symmetry of **12b**, in which the two NO ligands are indistinguishable from each other.

Table 1 gives an overview of the metrical data from the X-ray analyses. Two compounds, **8** and **12**, were found in both conformations. For **8**, crystals of the *vOC*-5 form **8a** were accompanied by a minor polymorph, the *TBPY*-5 conformer **8b**. In the case of **12**, both conformers, the *vOC*-5 form **12a** and the *TBPY*-5 conformer **12b** co-crystallise in the same solid.

The result of the continuous-shape-measures analysis is shown in Fig. 14. The assignment of a particular compound to one of the groups succeeded satisfactorily on a mere structural basis with a single exception: the data point for the Br/PPh_3 derivative **2** is found close to the *TBPY*-5 group but is assigned a *vOC*-5-type complex in a combined structural/spectroscopic view (Fig. 13).

IR spectroscopy

The structural differences between the *vOC*-5 and the *TBPY*-5 group are mirrored in the excitation-energy difference of the symmetrically and asymmetrically coupled N–O stretches. In the case of *vOC*-5, the $\Delta\nu$(NO) values show a large difference (71–157 cm^{-1}, solid state). Considerably smaller differences (28–41 cm^{-1}, solid state) characterise the *TBPY*-5 group (for all

Table 1 Metric data (exp.: crystal structure analysis, calc: DFT calculation). Details regarding the **a**/**b** issue: **7a**/**b** denote two independent *TBPY*-5-type molecules in the crystals' asymmetric unit; the DFT calculation converged to the same conformation. **8a** is the major *vOC*-5 isomer which is the minimum structure in the DFT calculation with or without considering a solvent model, **8b** is the minor *TBPY*-5 isomer which needed a solvent model to converge to a local minimum structure; **8b** is unstable by 1.4 kJ mol^{-1} referred to **8a** on the BP/tzvp + COSMO(CH_2Cl_2) level of theory. **12a**/**b** are the *vOC*-5/*TBPY*-5 conformer as found in crystals of [**12**]BF_4 at an equimolar ratio. Both conformers resemble local minima on the cation's hypersurface, **12a** being the stable one by 2.8 kJ mol^{-1} (BP/tzvp without a solvent model). Parameters that describe the actual conformation (Addison's τ_5-values and Alvarez's continuous shape measures are tabulated in the ESI.)

		Ru–N1–O1/°	Ru–N2–O2/°	ΔRu–N–O/°		Ru–N1/Å	Ru–N2/Å	ΔRu–N/Å
	PR_3/X	exp.	exp.	exp.	calc.	exp.	exp.	exp.
1	PPh_3/Cl	178.9(2)	134.8(2)	44.1	39.1	1.746(2)	1.872(2)	0.126
2	PPh_3/Br	175.3(3)	143.1(2)	32.2	35.1	1.753(2)	1.854(2)	0.101
3	PPh_2Bn/Cl	167.2(2)	164.0(2)	3.2	5.5	1.781(2)	1.785(2)	0.004
4	PPh_2Bn/Br	168.3(3)	162.4(3)	5.9	7.0	1.776(3)	1.781(3)	0.005
5	PCy_3/Cl	179.9(3)	136.5(2)	43.4	39.1	1.739(3)	1.870(3)	0.131
6	PCy_3/Br	177.3(6)	139.3(6)	38.0	37.8	1.756(6)	1.846(6)	0.090
7a	PCy_3/I	170.9(8)	165.9(8)	5.0	4.7	1.773(8)	1.789(9)	0.016
7b	PCy_3/I	170.3(9)	163.1(8)	7.2	4.7	1.791(9)	1.790(7)	0.001
8a	$PCyp_3$/Cl	176.9(4)	137.0(4)	39.9	39.7	1.758(3)	1.850(4)	0.092
8b	$PCyp_3$/Cl	168.1(2)	164.4(2)	3.7	9.7	1.775(2)	1.783(2)	0.008
9	$PCyp_3$/Br	168.7(3)	166.6(3)	2.1	5.4	1.779(3)	1.780(3)	0.001
10	$PCyp_3$/I	168.9(4)	165.5(4)	3.4	5.3	1.779(4)	1.787(4)	0.008
11	P^iPr_3/Cl	178.0(9)	149.2(8)	28.8	38.3	1.740(8)	1.831(8)	0.091
12a	P^iPr_3/Br	177(1)	150.8(3)	26.2	41.2	1.72(1)	1.860(5)	0.140
12b	P^iPr_3/Br	165.34(3)	165.34(3)	0.0	0.5	1.785(3)	1.785(3)	0.000

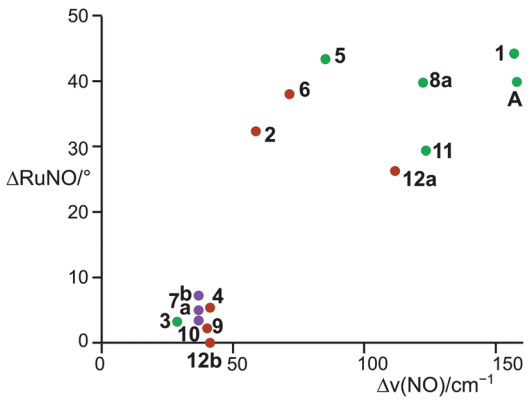

Fig. 13 Adopted structures (bottom left group: *TBPY*-5, top right data points: *vOC*-5) depending on the Ru–N–O angle and the ν(NO) stretching frequency. Colour code: purple (X = I), reddish brown (X = Br), green (X = Cl).

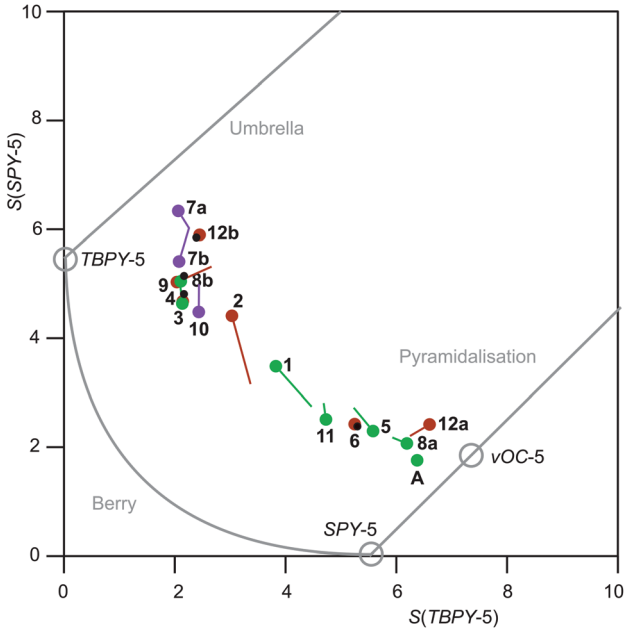

Fig. 14 Shape map for pentacoordinate complex ions $[Ru(NO)_2(PR_3)_2X]^+$. The graph was drawn by using Fig. 6 of ref. 23 as a template (from which the commentary printed in grey was transferred as well). Purple (X = I), reddish brown (X = Br) and green (X = Cl) circles are drawn at the experimental values; lines of the respective colour end at the DFT-calculated values; small black circles within larger coloured circles indicate that the DFT value gave a data point within the experimental value's circle radius.

ranges and mean values, **2**, which was correctly assigned in the combined map of Fig. 13, was not included). IR spectra of crystals of **12**, which contained the *vOC*-5 and *TBPY*-5 conformers in equal parts, provided us with useful information for the interpretation of solution spectra: for a *vOC*-5 conformer, the symmetrically coupled vibration is dominated by the linearly bonded ligand (see the DFT part below) and reaches the highest excitation energy. The symmetrically coupled vibration of the *TBPY*-5 conformer is observed at a somewhat lower excitation energy. However, the two symmetrically coupled stretches may appear so close in the spectrum that they may overlap, at least at higher temperatures (Fig. 15). The asymmetrically coupled nitrosyl stretches are well resolved with the lower frequency for the *vOC*-5 conformer whose lower-energy stretch is dominated by the $^{1}NO^{-}$ ligand. As a result, three to four bands are observed in the case of compounds that exhibit both conformations, the couple of *TBPY*-5 bands ("b" in Fig. 15) being nested in the band couple of the *vOC*-5 form ("a" in Fig. 15).

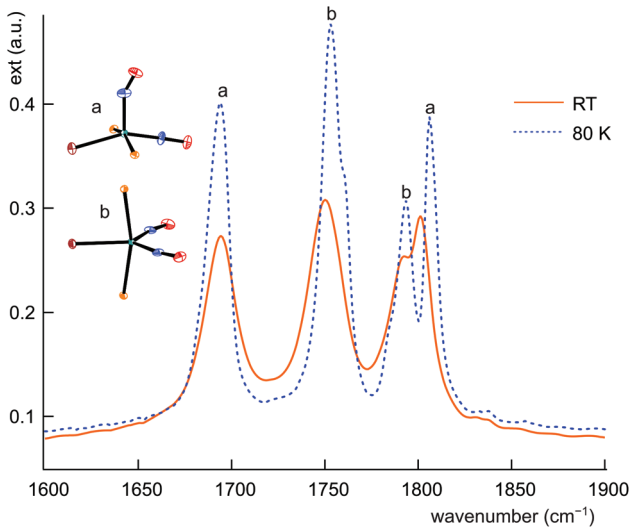

Fig. 15 IR spectrum of the ground state of **12a/b** in the ν(NO) range at RT (solid line) and 80 K (dashed line).

The clear-cut difference between the asymmetrically coupled stretches allows for the interpretation of the whole body of data of Table 2. The dissolution of crystals of **12** in dichloromethane results in the transformation of the *vOC*-5 conformer to the *TBPY*-5 form as the only conformer in solution. In the case of **1**, **6**, **8**, and **11**, dissolution in CH_2Cl_2 induces the formation of a mixture of the conformers. The full set of bands was resolved for **8**, whereas the coincidence of the symmetrically coupled stretches was observed for **1**, **6**, and **11**. (For a solution of **A** in methanol, four bands had been observed.[15])

The combination of the crystallographical and the spectroscopical analysis allows for a reliable assignment of a conformation in question. Fig. 13 shows two clearly resolved fields of existence of the conformers, a narrow field for the *TBPY*-5 group and a broader one for the *vOC*-5 conformer.

DFT calculations

Both the metrical as well as the spectroscopical data are satisfyingly reproduced by calculation in the framework of density functional theory (compare the "calc." entries in Tables 1 and 2). In Fig. 14, the computational results are sketched in as well. The resemblance of experimental and calculated values is mostly satisfactory. Larger deviations ensued for the PPh_3/Cl (**1**) and the PPh_3/Br (**2**) couples only. The τ_5 values from calculation and experiment show a maximum deviation of 0.10, found for **2**.

In terms of frequencies, the measured values in the solid and liquid states are in relatively good agreement with those calculated as well. If the calculated frequencies and the frequencies measured in solid samples are compared, it is obvious that the asymmetric vibration tends to be predicted a bit too high, the mean deviation being +12.9 cm^{-1} [$\Delta\nu$(NO) = $\nu(NO)_{calcd} - \nu(NO)_{exp.}$], whereas the symmetric vibration mode is predicted more reliably ($\Delta\nu$(NO) = +1.8 cm^{-1}). It should be noted that all DFT-derived frequencies are listed without applying a correction factor.

A slightly better agreement between calculated and observed frequencies was found for the liquid state values that are devoid of contributions from specific intermolecular interactions. Specifically, the uncorrected asymmetric vibration was predicted slightly too high ($\Delta\nu$(NO) = 2.5 cm^{-1}), and the symmetric vibration mode was predicted slightly too low ($\Delta\nu$(NO) = −1.83 cm^{-1}).

For **8**, both the *vOC*-5 and the *TBPY*-5 forms were found in the solid state, the *vOC*-5 conformer **8a** as the major form, with an admixture of a few crystals of **8b** (hence, no solid-state IR data are given for **8b** in Table 2). On attempts to model both

Table 2 Spectroscopic data (symmetric/asymmetric N–O stretch; solid: ATR-IR of crystalline samples, CH_2Cl_2: dichloromethane solution, DFT: DFT calculation)

	PR_3/X	$\nu(NO)_{sym,asym}$/cm^{-1} Solid	$\nu(NO)_{sym,asym}$/cm^{-1} DFT	$\nu(NO)_{sym,asym}$/cm^{-1} CH_2Cl_2	$\Delta\nu$(NO)/cm^{-1} Solid/calc.	Conformation (Solid)
1	PPh_3/Cl	1842/1685	1830/1724	1823/1776/1720[a,b,c]	157/106	*vOC*-5
2	PPh_3/Br	1824/1765	1819/1736	1813/1778	59/83	*vOC*-5
3	PPh_2Bn/Cl	1799/1771	1811/1788	1818/1776	28/23	*TBPY*-5
4	PPh_2Bn/Br	1817/1776	1809/1787	1815/1778	41/22	*TBPY*-5
5	PCy_3/Cl	1789/1704	1806/1709	1812/1706	85/97	*vOC*-5
6	PCy_3/Br	1785/1714	1799/1709	1800/1760/1716[a,b,d]	71/90	*vOC*-5
7	PCy_3/I	1788/1751	1791/1768	1797/1765	37/23	*TBPY*-5
8a	$PCyp_3$/Cl	1805/1681	1809/1710	1834/1797/1754/1710[a,d]	124/99	*vOC*-5
9	$PCyp_3$/Br	1810/1770	1809/1783	1795/1759	40/26	*TBPY*-5
10	$PCyp_3$/I	1809/1772	1793/1769	1794/1759	37/24	*TBPY*-5
11	P^iPr_3/Cl	1808/1682	1815/1717	1809/1759/1714[a,b,c]	126/98	*vOC*-5
12a	P^iPr_3/Br	1806/1694[e]	1809/1710	1802/1765[f]	112/99	*vOC*-5
12b	P^iPr_3/Br	1794/1753[e]	1799/1776	1802/1765	41/23	*TBPY*-5

[a] *TBPY*-5/*vOC*-5 conformational mixture in solution; *cf.* ref. 15. [b] Coincidence of the symmetric N–O stretches of the two conformations at the maximum of the three values. [c] No local minimum found for the *TBPY*-5 conformer in the DFT calculation both with and without COSMO approach to solvation. [d] Local minimum for the *TBPY*-5 conformer found for the COSMO(CH_2Cl_2) calculation; calculated frequencies/cm^{-1} (*TBPY*-5 values in italics): **6** 1791, *1780*/*1745*/1691, **8a**/**b** 1800/*1795*/*1766*/1688. [e] Frequencies measured on a Nicolet 5700 FTIR device for the sake of its better spectral resolution (2 cm^{-1}). [f] Transformation of the *vOC*-5 conformer to *TBPY*-5 on dissolution.

conformers using the standard procedure (no solvent model applied), only **8a** was found as a minimum structure, whereas **8b** converged into **8a** on refinement. However, a local minimum was obtained for **8b** also by the application of a COSMO model with the parameters of dichloromethane. **8a** also remained a minimum structure in the COSMO calculations, the energetic difference of both conformers being rather small (1.4 kJ mol^{-1} instability of **8b**), in line with the common occurrence of both conformers in solution spectra.

For **12**, both conformations were local minima on the conformational hypersurface in the standard as well as the COSMO-DFT treatment with the *vOC*-5 conformer the global minimum, and the *TBPY*-5 at some 3 kJ mol^{-1} less stable for **12.**

Though two crystallographically confirmed conformers were found for **8** and **12** only, IR spectra of solutions of the *vOC*-5 species **1**, **6**, and **11** revealed the existence of their *TBPY*-5 counterparts. However, with or without the application of the COSMO solvent model, we did not succeed in locating a minimum structure for a *TBPY*-5 isomer with the specified methods and basis sets for **1** and **11.** For **6**, however, both the COSMO and the pure gas-phase approach led to local minima for the two conformations. As expected for the IR result, the stability of both conformers was practically equal (*TBPY*-5 instable by 1.1 and 1.4 kJ mol^{-1} for the gas-phase and the COSMO refinement, respectively).

The distribution of the conformers is summarised in Table 3. Dinitrosyl complexes with the *vOC*-5 structure are primarily found on the top left, compounds which adopt both structures in the middle, and compounds adopting the *TBPY*-5 structure bottom right.

Bonding in the $[RuX(NO)_2(PR_3)_2]^+$ cations

The argumentation used in the following attempt to rationalise the experimental results agrees with qualitative molecular-orbital considerations published by Enemark and Feltham and by Hoffmann and Rossi some four decades ago.[2,26] As shown before, the observed conformation is obviously correlated to the coordination entity's electronic situation. Thus, **A**, **1**, **2**, **5**, **6**, **8a**, **11** and **12a**, all of which adopt the *vOC*-5 conformation, constitute a group of less electron-rich species in terms of the kind of halide and Tolman's parameter of the phosphane. **3**, **4**, **7**, **8b–10** and **12b** adopt the *TBPY*-5 structure in agreement with the higher electron supply of the heavier halides and/or the more electron-donating phosphanes.

Table 3 Structure of the cation in $[RuX(NO)(PR_3)_2]BF_4$ compounds in the solid depending on X and R. Deviating results for the solution state are printed bold. The electronic parameter of the phosphanes [ν(CO) according to Tolman] decreases from left to right, indicating increasing donor strength in that direction. The donor ability of the halides increases from top to bottom, resulting in increasing electron-density supply at the metal centre from top left to bottom right

	PPh_3	P^iPr_3	PCy_3	$PCyp_3$
Cl	*vOC*-5 **+*TBPY*-5**	*vOC*-5 **+*TBPY*-5**	*vOC*-5	*vOC*-5 + *TBPY*-5
Br	*TBPY*-5	*vOC*-5 + *TBPY*-5 **only**	*vOC*-5 **+*TBPY*-5**	*TBPY*-5
I		*TBPY*-5	*TBPY*-5	*TBPY*-5

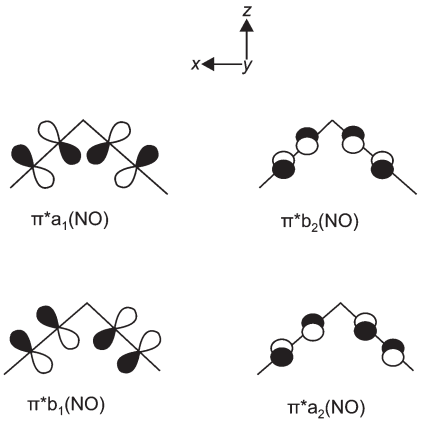

Fig. 16 The ligand group orbitals in C_{2v} symmetry derived from the π* orbitals of the two NO ligands. Adapted from ref. 2.

The fact that a square-planar conformer with one bent nitrosyl, and a trigonal bipyramidal conformer with more or less linear nitrosyls are the two alternatives for five-coordinate $\{M(NO)_2\}^8$ species had been recognised by Enemark and Feltham prior to the discovery of a first representative of the *TPBY*-5 type.[2] Their analysis starts with the presentation of the four combinations of the NO-π* orbitals in a *cis*-$M(NO)_2$ fragment. Fig. 16 shows, for the point group C_{2v}, these four ligand group orbitals which represent the nitrosyl ligands' contribution to the frontier orbital range. As a starting point for the discussion, an idealised conformation was considered with a 90° N–M–N angle and linear M–N–O fragments. In this situation, the a_1, a_2 and b_2 orbitals are metal–ligand-bonding by their interaction with the $x^2 - z^2$, *xy* and *yz* metal d-orbitals, respectively. Moreover, these three molecular orbitals remain metal–ligand bonding in the course of distorting the depicted starting conformation and thus are filled for all conformations in question with six of the eight electrons of the $\{M(NO)_2\}^8$ moiety. The ligand b_1 orbital, however, is orthogonal to the metal d orbital of the same symmetry (*xz*) in the virtual starting conformation. To remove this loss of stability, Enemark and Feltham considered, depending on the overall electron supply, two possible distortions that provide a metal–ligand bonding molecular orbital also for the remaining two electrons. Fig. 17, re-drawn from ref. 2, shows the two considered distortional paths that stabilise this electron pair. From the metal's viewpoint, the right part of Fig. 17 treats the electron-rich variant with all eight electrons metal centered. Here, the b_1 electron pair is positioned in the metal *xz* orbital [Fig. 17(c)]. To make the orthogonal metal–ligand contact of Fig. 17(c) metal–ligand-bonded, the N–M–N angle increases [Fig. 17(d)] and some degree of bonding overlap is achieved (the mean N–Ru–N angle for the *TBPY*-5 species of this work is 117.4°). As a result, the electron-rich *TBPY*-5 complexes reported herein are interpreted as d^8-ruthenium(0) centres with two formal NO^+ ligands.

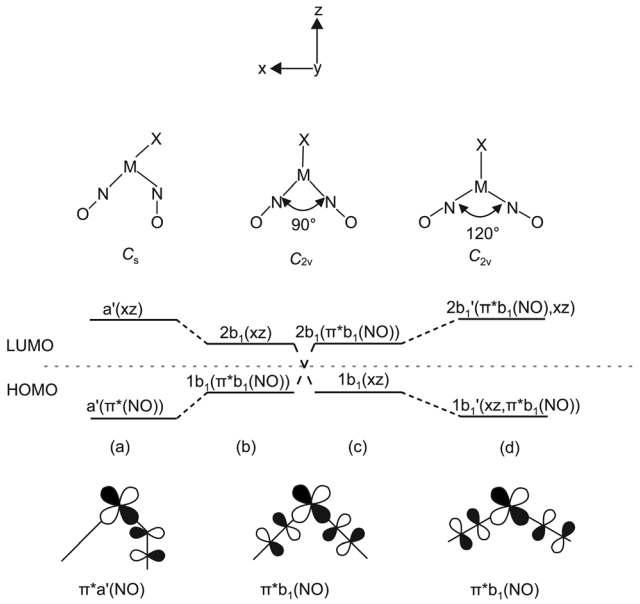

Fig. 17 Left: Correlation diagram showing the proposed behaviour of the $1b_1$ and $2b_1$ molecular orbitals in five-coordinate $\{M(NO)_2\}^8$ complexes with a $(1b_1)^2$ electron configuration. Scheme (b) has $\pi^*b_1(NO)$ lower in energy than d_{xz} and leads to structure (a). Scheme (c) has d_{xz} lower in energy than $\pi^*b_1(NO)$ and leads to (d). Adapted from ref. 2 Bottom: The relevant HOMO which is metal–ligand non-bonding at an N–M–N angle of 90°.

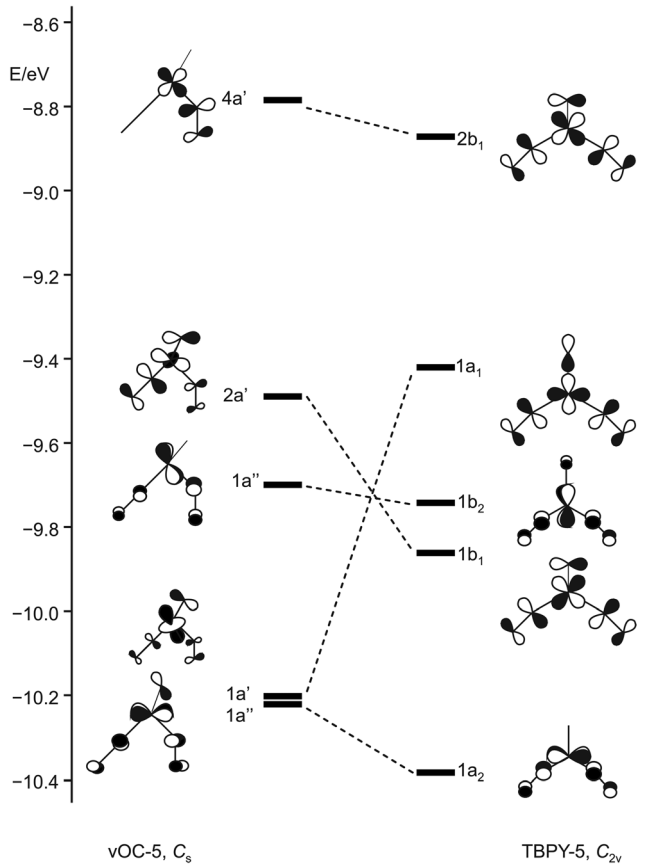

Fig. 18 Schematic representation of selected frontier orbitals for the C_{2v} (*TBPY*-5) and the C_s (*vOC*-5) conformer of **12** calculated by a DFT-based method.

In the metal-electron-poor variant, Enemark and Feltham placed the two electrons in question in the ligand-centered b_1 orbital [Fig. 17(b)]. The system relaxes by a bend of one of the nitrosyl ligands, thus lowering the symmetry to C_s [Fig. 17(a)]. Metal–ligand bonding is achieved *via* the overlap of the respective orbital of a formal $^1NO^-$ ligand and the metal-d(*xz*) orbital with local σ symmetry. Hence, in the more electron-poor complexes of this work, d^6-ruthenium(II) centres are bonded to a $NO^+/^1NO^-$ nitrosyl couple.

Enemark and Feltham's qualitative discussion is supported by our DFT calculations. Fig. 18 shows the result for the C_s-symmetric *vOC*-5 conformer **12a** and the C_{2v}-symmetric *TBPY*-5 conformer **12b**. Both conformers present energetic minima that assure metal–ligand bonds for all four electron pairs of the $\{Ru(NO)_2\}^8$ configuration, even for the least stable b_1/a' pair.

Photophysical investigation of $[RuBr(NO)_2(P^iPr_3)_2]BF_4$ (12)

Dinitrosyl complexes promise to be particularly interesting objects for photophysical research on the linkage isomer issue since they provide a larger number of excitation and decay pathways than mononitrosyl compounds – if they are excitable at all. To check the principal suitability of $\{Ru(NO)_2\}^8$ compounds for the formation of metastable linkage isomers *via* photoexcitation, we chose **12** since both conformers **12a** and **12b** are present at an equal ratio in crystals of the tetrafluoridoborate.

To test under which conditions the population of metastable isomers is achievable, **12** was irradiated with laser light of the wavelengths 405, 445 and 476 nm at 80 K. The maximal photo-excitation was reached at 405 nm. Fig. 19 shows an infrared spectrum in the ν(NO) range of the ground state and the photo-excited state at 80 K. Upon illumination in the blue spectral range, the two conformers reacted differently with the *vOC*-5 conformer showing the more distinct change. Hence, the two NO stretches of **12a** (1806 and 1694 cm^{-1} in the ground state) were affected most and lost about 70% of their intensity. New absorption bands appeared at 1649 and 1821 cm^{-1}, −45 cm^{-1} relative to the asymmetrically coupled stretch, and +15 cm^{-1} relative to the symmetrical stretching mode (blue spectrum in Fig. 19). The ground-state bands of the *TBPY*-5 isomer **12b** were much less affected on irradiation. A decay of about 30% is apparent but no new bands of matching intensity were observed. The photo-switching is reversible: irradiation with red light (660 nm) restored most of the original spectrum (Fig. 19), complete restoration of the initial state was observed on warming the samples (Fig. 20). Since the asymmetrically coupled, $^1NO^-$-dominated absorption band of **12a** experienced the largest shift, we see this ligand of the four different nitrosyls of **12** as the switched one. The smaller shift of the linearly bonded NO ligand of **12a** would thus simply mirror the altered bonding situation within the bent Ru–N–O moiety in the photoinduced isomer of **12a**.

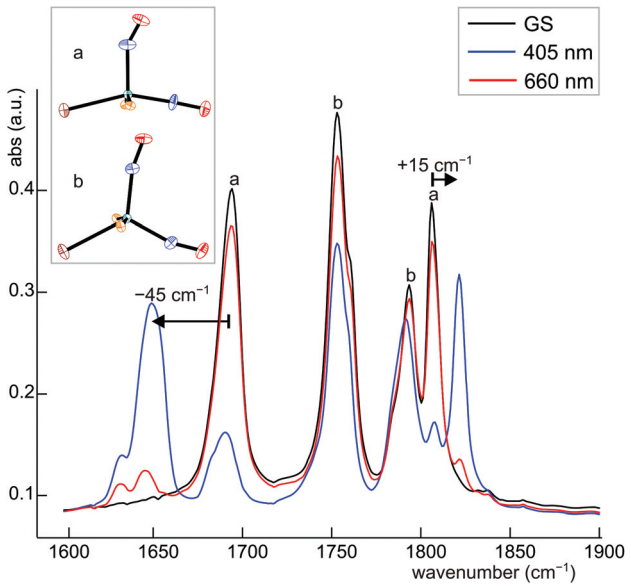

Fig. 19 IR spectrum of **12a/b** in the ν(NO) range before (black line) and after population (405 nm, blue line) and depopulation (606 nm, red line) by irradiation with light of the appropriate wavelength at 80 K.

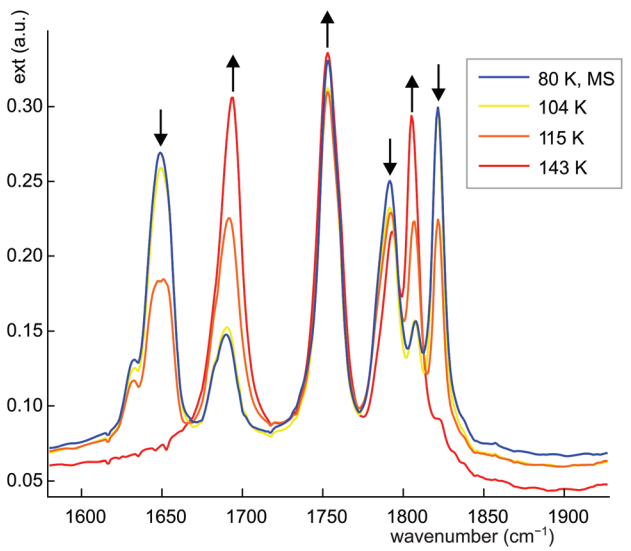

Fig. 20 IR spectrum of **12a/b** in the ν(NO) range after population at 80 K and subsequent thermal depopulation by gradual heating (yellow, orange and red line), the arrows indicate the change upon warming.

No attempts were made in this report to investigate the characteristics of the metastable state in detail. Work on this issue is in progress and will be reported in due course.

Conclusions

Eleven compounds of the $\{Ru(NO)_2\}^8$ type were synthesised by slightly modified procedures adopted from Townsend and Ibers.[27,28] The dinitrosyl complexes of the general formula $[RuX(NO)_2(PR_3)_2]BF_4$ (X = Cl, Br, I; PR_3 = PPh_3, PPh_2Bn, PCy_3, $PCyp_3$, P^iPr_3) were characterised by X-ray diffraction and spectroscopic methods (IR, NMR), mass spectrometry and elemental analysis. X-ray studies of the dinitrosyl compounds reveal that they adopt two different structures: one which was already known for $\{Ru(NO)_2\}^8$ compounds, and another one which has, so far, been unknown for ruthenium dinitrosyls but has been found for an osmium homologue. The known structure is of the vacant-octahedron type (*vOC*-5) in terms of continuous shape measures (CShM);[23] the maximum possible symmetry is C_s. It shows two distinct bonding modes for the two NO ligands, a formal NO^+ and a formal $^1NO^-$ group. Animations of the calculated ν(NO) vibrations reveal that, of the two N–O stretches, the higher-energy symmetrically coupled vibration is dominated by the linearly coordinated nitrosyl and the lower-energy asymmetrically coupled vibration by the bent-coordinated nitrosyl ligand. The extent of vibrational coupling is higher in the second group of complex cations which adopt a trigonal bipyramidal structure (*TBPY*-5) in terms of CShM values; the maximum possible symmetry is C_{2v}. The coordination entities show an equal bonding situation for the two NO ligands. This structure, predicted in a review article by Enemark and Feltham for five-coordinate $\{M(NO)_2\}^8$ compounds of third-row transition metals and good π-accepting ligands X, is known for M = Re, Mn and X = Cl, CO, and, more closely to the compounds of this work, for the osmium homologue of **1**, $[OsCl(NO)_2(PPh_3)_2]BF_4$ (it might be noted that Enemark and Feltham's bonding analysis was correct but their prediction regarding the occurrence of the *TBPY*-5 form was not).[16] Animations of the calculated ν(NO) vibrations of the compounds with this structure reveal, as expected, equal contributions of both N–O stretches to the symmetrically and the asymmetrically coupled vibrations at higher and lower excitation energy, respectively.

All structures were verified by DFT calculation, both in terms of structural data and vibrational frequencies. The actually developed structure type depends, primarily, on the nature of X, and, secondarily, on the substituent R of the phosphane. Both structure types for the same compound were found experimentally for the complex cations of $[RuBr(NO)_2(P^iPr_3)_2]BF_4$ (**12**) and $[RuCl(NO)_2(PCyp_3)_2]BF_4$ (**8**) in the solid state, and, in dichloromethane solution, for **1**, **6**, **8**, and **11** (as a peculiarity, both conformers of **12** are transformed to the *TBPY*-5 form **12b** on dissolution in CH_2Cl_2).

The frontier orbitals of the two conformers of **12** were compared with the predictions made by Enemark and Feltham for square planar and trigonal bipyramidal pentacoordinate $\{M(NO)_2\}^8$ compounds.[2] Although *TBPY*-5 compounds of this type were not known at that time, and the predictions were, thus, based only on symmetry and overlap criteria, the energetic order as well as the type of orbitals involved are, to a great extent, consistent with the DFT results.

Generally, the *vOC*-5 structure is found preferentially for the chlorido species, whereas the iodido compounds are the realm of the *TBPY*-5 type. Thus, we conclude that the adopted structure is primarily dominated by the halogenido ligand and,

secondarily, by Tolman's electronic factor of the phosphane ligand (Table 3, Fig. 14). Obviously, the occurrence of any of the two conformers mirrors the electronic supply by the halogenide and the phosphane. In a simplifying view, the *TBPY*-5 class is consistent with the electron-rich situation of d^8-Ru^0 centres that bind two NO^+ ligands. Less electron-rich complexes switch to a bent coordination of one nitrosyl ligand. These, in the ideal case, C_s-symmetrical compounds can be regarded as derivatives of d^6-Ru^{II} centres coordinating to one NO^+ and one $^1NO^-$ ligand.

An orienting investigation on the photo-excitability was conducted for **12** for which both conformers are present within the same crystal structure at equal parts. As a preliminary result, a high degree of population of the metastable, $^1NO^-$-switched state was found for the *vOC*-5 conformer on irradiation with blue light.

After having demonstrated the photo-excitability of $\{Ru(NO)_2\}^8$ compounds, photo-physical investigations including photo-crystallographic experiments as well as quantum-chemical calculations of the metastable states are currently in progress and will be reported in a separate work.

Experimental

Materials

$RuCl_3{\cdot}xH_2O$ was purchased by Alfa Aesar or ABCR. Benzyldiphenylphosphane, tricyclohexylphosphane and tri-isopropylphosphane were used as supplied by ABCR. HBr (48%), Zn_nCu and triphenylphosphane were purchased by ACROS Organics. Tricyclopentylphosphane, $NOBF_4$ and toluene (kept over molecular sieve) were purchased by Sigma-Aldrich. KNO_2 and HCl (37%) were used as supplied by Fluka. Diethyl ether, ethanol and HI (57%) were purchased from Merck. 1 M HCl was used as supplied by AppliChem. Ethanol was dried over molecular sieve and degassed. Water used for the preparation of the phosphane-containing mononitrosyl compounds, and toluene were also degassed. $K_2[RuCl_5(NO)]$, $K_2[RuBr_5(NO)]$, $K_2[RuI_5(NO)]$, $[RuCl_3(NO)(PPh_3)_2]$ were prepared according to the literature.[19,29,30] $[RuCl(NO)_2(PPh_3)_2]BF_4$ was prepared by a slightly modified literature procedure. The synthesis as well as the consecutive reaction of the precursor compounds of the general formula $[RuX_{1-3}(NO)(PR_3)_2]$ were performed using standard Schlenk technique, since the compounds are air-sensitive, unless $X = 3$. The $\{RuNO\}^6$ as well as the $\{Ru(NO)_2\}^8$ compounds are air-stable.

General information

Standard procedures are specified in the ESI.†

Computational details

All calculations were performed with the ORCA 3.0 program package. Structures were optimised with the Becke-Perdew density (BP) method and the Ahlrichs-type basis set tzvp for all atoms except ruthenium and iodine. Found stationary points were confirmed with subsequent frequency analyses on the corresponding level of theory, except that no ECPs were used. Instead, scalar relativistic all-electron calculations were performed for ruthenium and iodine.[31] Continuous shape measures were calculated with the programme SHAPE.[23,32]

IR spectroscopy at low temperature

Measurements of IR spectra at low temperatures were performed using a Nicolet 5700 FTIR spectrometer. The powdered samples were mixed with KBr and pressed into pellets. The KBr pellets were mounted on a copper cold finger using silver paste for good thermal contact. The samples were cooled to 85 K in a liquid nitrogen cryostat. KBr windows allowed the irradiation of the sample with laser light and absorption measurements down to 390 cm^{-1}. Irradiation was performed with lasers as described above.

Synthesis

General aspects. Since the phosphanes PCy_3, $PCyp_3$ and P^iPr_3 are sensitive towards oxidation, mononitrosyl complexes with these ligands were prepared under inert-gas atmosphere. In contrast to the mononitrosyls containing PPh_3 or PPh_2Bn as ligands, the complexes of the stronger reducing phosphanes were isolated as $\{RuNO\}^n$ mixtures with n = 6–8 (several signals in the NMR spectrum and several peaks in the region assignable to coordinated nitrosyl in the IR spectrum). Therefore no data derived from elemental analysis are provided except in two cases for which a yield could be specified, as the elemental analysis of the product is in agreement with a formulation of the product as a pure $\{RuNO\}^7$ compound. The m/z ratio of the mass spectra of the $\{RuNO\}^n$ mixtures are calculated with regard to a $\{RuNO\}^7$ compound of the formula $[RuX_2(NO)(PR_3)_2]$. The phosphane-containing mononitrosyl compounds were used, without further purification, in the consecutive reaction, yielding the dinitrosyl since the $\{RuNO\}^n$ mixtures were uniformly reduced with Zn_nCu to the respective $\{RuNO\}^8$ compound.

$[RuBr_3(NO)(PPh_3)_2]$. Triphenylphosphane (1.57 g, 6.00 mmol), dissolved in hot ethanol (10 mL), was added to a water–ethanol solution (1/1 mixture, 20 mL) of dipotassium pentabromidonitrosylruthenate (1.22 g, 2.00 mmol) and was heated under reflux for 45 min. During the reaction an orange-brown solid was formed, which was filtered off after cooling to room temperature. Subsequently the raw product was washed with ethanol and diethyl ether and dried *in vacuo*. Yield: 1.46 g, 1.64 mmol, 81.8%. ^{31}P NMR (109 MHz, C_7H_8, 25 °C) δ/ppm: 25.0. Selected IR bands ν_{max}/cm^{-1}: 1870 (s, NO), 1480 (m), 1435 (s), 1192 (w), 1163 (w), 1090 (s), 997 (w), 741 (s), 703 (s), 688 (vs). Elemental analysis (%): calc. C 48.29, H 3.38, N 1.56; found: C 48.79, H 3.40, N 1.61.

$[RuCl_3(NO)(PPh_2Bn)_2]$. An ethanolic solution (5 mL) of ruthenium nitrosyl chloride hydrate (0.453 g, 1.78 mmol) was added to benzyldiphenylphosphane (1.23 g, 4.44 mmol), dissolved in hot ethanol (5 mL), and heated under reflux for 20 minutes. The yellow-orange solid formed during the reaction was separated by filtration, washed with a 1 : 1 : 2 mixture of dichloromethane–ethanol–*n*-hexane (12 mL) and dried

in vacuo. Yield: 1.26 g, 1.59 mmol, 89.3%. ^{31}P NMR (109 MHz, C_7H_8, 25 °C) δ/ppm: 19.6. Selected IR bands ν_{max}/cm^{-1}: 1850 (s, NO), 1599 (vw), 1495 (w), 1482 (w), 1453 (w), 1433 (m), 1408 (w), 1330 (w), 1185 (w), 1143 (w), 1094 (w), 1096 (w), 1030 (w), 1000 (w), 914 (w), 831 (m), 773 (m), 752 (m), 740 (s), 697 (s). MS-FAB (NBA): *m*/*z* calcd 754.1 for $[RuCl_2(NO)(PPh_2Bn)_2]^+$ = $[M - Cl]^+$, found 754.0. Elemental analysis (%): calc. C 57.77, H 4.34, Cl 13.46, N 1.77; found: C 58.05, H 4.44, Cl 13.13, N 1.64.

[RuBr$_3$(NO)(PPh$_2$Bn)$_2$]. Benzyldiphenylphosphane (0.481 g, 1.74 mmol), dissolved in hot ethanol (5 mL), was treated with a solution of dipotassium pentabromido nitrosyl ruthenate (0.424 g, 0.696 mmol) in ethanol–water (3 : 1, 10 mL) and heated under reflux for 30 minutes. In the course of the reaction a yellow-orange solid precipitated which, after cooling to room temperature, was filtered off and washed with a mixture of ethanol–dichloromethane–*n*-hexane (1 : 1 : 2). The product was freed from all volatile components *in vacuo.* Yield: 0.610 g, 0.661 mmol, 94.3%. ^{31}P NMR (109 MHz, C_7H_8, 25 °C) δ/ppm: 12.9. Selected IR bands ν_{max}/cm^{-1}: 1847 (s, NO), 1494 (vw), 1453 (vw), 1432 (w), 1408 (vw), 1143 (vw), 1099 (vw), 1069 (vw), 1030 (vw), 830 (m), 772 (m), 750 (m), 739 (s), 697 (vs). MS-FAB (NBA): *m*/*z* calcd 844.0 for $[RuBr_2(NO)(PPh_2Bn)_2]^+$ = $[M - Br]^+$, found 844.0. Elemental analysis (%): calc. C 49.43, H 3.71, N 1.52; found: C 50.58, H 3.83, N 1.30.

[RuCl$_{1-3}$(NO)(PCy$_3$)$_2$]. Dipotassium pentachlorido nitrosyl ruthenate (1.14 g, 2.94 mmol), dissolved in ethanol–water (1 : 1, 60 mL), was added to a solution of tricyclohexylphosphane (2.06 g, 7.35 mmol) in hot ethanol (55 mL). The reaction mixture was kept under refluxing conditions for 4 hours. The resulting solid was collected by filtration and dried *in vacuo.* Yield: 1.67 g. ^{31}P NMR (109 MHz, C_7H_8, 25 °C) δ/ppm: 38.8, 25.2, 17.6. Selected IR bands ν_{max}/cm^{-1}: 2921 (vs), 2846 (vs), 1826 (vs), 1802 (w), 1712 (vs), 1442 (s), 1264 (m), 1195 (m), 1173 (s), 1127 (w), 1002 (s), 899 (m), 847 (s), 734 (m). MS-FAB (NBA): *m*/*z* calcd for $C_{36}H_{66}ClNOP_2Ru$ = $[M]^+$ 762.3045, found 762.3013; $[M - Cl]^+$ 727.3359, found 727.3315.

[RuBr$_{1-3}$(NO)(PCy$_3$)$_2$]. Dipotassium pentabromido nitrosyl ruthenate (1.00 g, 1.64 mmol), dissolved in ethanol–water (1 : 1, 70 mL), was added to a solution of tricyclohexylphosphane (1.15 g, 4.11 mmol) in hot ethanol (50 mL). The reaction mixture was kept under refluxing conditions for 1 hour. The resulting green solid was collected by filtration, washed with ethanol–dichloromethane–*n*-hexane (1 : 1 : 2, 28 mL) and dried *in vacuo.* Yield: 1.00 g. ^{31}P NMR (109 MHz, C_7H_8, 25 °C) δ/ppm: 73.7, 36.5, 24.8, 16.2, 9.3. Selected IR bands ν_{max}/cm^{-1}: 2922 (vs), 2846 (m), 1825 (w), 1802 (m), 1752 (w), 1709 (s), 1442 (m), 1265 (vw), 1172 (m), 1127 (vw), 1001 (m), 886 (w), 846 (m), 732 (m). MS-FAB (NBA): *m*/*z* calcd for $C_{36}H_{66}BrNOP_2Ru$ = $[M]^+$ 852.2023, found 852.2046; $[M - Br]^+$ 773.2888, found 773.2847.

[RuI$_{1-3}$(NO)(PCy$_3$)$_2$]. Dipotassium pentaiodido nitrosyl ruthenate (0.72 g, 0.85 mmol), dissolved in ethanol–water (2 : 1, 24 mL), was added to a solution of tricyclohexylphosphane (0.62 g, 2.2 mmol) in hot ethanol (17 mL). The reaction mixture was kept under refluxing conditions for 1 hour. The resulting green solid was collected by filtration, washed with ethanol–dichloromethane–*n*-hexane (1 : 1 : 2, 28 mL) and dried *in vacuo.* Yield: 0.23 g. ^{31}P NMR (109 MHz, C_7H_8, 25 °C) δ/ppm: 45.8, 34.1, 25.6, 16.9, 11.3. Selected IR bands ν_{max}/cm^{-1}: 2923 (m), 2846 (m), 1798 (m, NO), 1756 (m, NO), 1706 (vs, NO), 1442 (m), 1297 (vw), 1264 (w), 1172 (m), 1002 (m), 886 (w), 845 (m), 814 (w), 731 (m), 652 (w). MS-FAB (NBA): *m*/*z* calcd for $C_{36}H_{66}INOP_2Ru$ = $[M - I]^+$ 819.27, found 820.0

[RuCl$_{1-3}$(NO)(PCyp$_3$)$_2$]. Dipotassium pentachlorido nitrosyl ruthenate (0.675 g, 1.75 mmol), dissolved in ethanol–water (1 : 1, 70 mL), was added to a solution of tricyclopentylphosphane (1.00 g, 4.20 mmol) in hot ethanol (10 mL). The reaction mixture was kept under refluxing conditions for 1 hour. The resulting solid was collected by filtration and dried *in vacuo.* Yield: 1.20 g. ^{31}P NMR (109 MHz, C_7H_8, 25 °C) δ/ppm: 39.2, 20.7, 17.9, 5.0. Selected IR bands ν_{max}/cm^{-1}: 2947 (m), 2863 (m), 1803 (m), 1703 (vs), 1447 (w), 1299 (w), 1230 (w), 1120 (w), 1011 (vw), 906 (w), 724 (vw), 619 (vw). MS-FAB (NBA): *m*/*z* calcd for $C_{30}H_{54}ClNOP_2Ru$ = $[M - Cl]^+$ 727.39, found 727.8.

[RuBr$_{1-3}$(NO)(PCyp$_3$)$_2$]. Dipotassium pentabromido nitrosyl ruthenate (1.06 g, 1.75 mmol), dissolved in ethanol–water (1 : 1, 70 mL), was added to a solution of tricyclopentylphosphane (1.00 g, 4.43 mmol) in hot ethanol (10 mL). The reaction mixture was kept under refluxing conditions for 1 hour. The resulting green solid was collected by filtration and dried *in vacuo.* Yield: 0.965 g, 1.14 mmol, 65%. ^{31}P NMR (109 MHz, C_7H_8, 25 °C) δ/ppm: 36.9, 27.1, 15.4, 15.0. Selected IR bands ν_{max}/cm^{-1}: 2954 (m), 2864 (w), 1828 (NO), 1806 (NO), 1762 (w), 1703 (m), 1447 (vw), 1298 (vw), 1259 (m), 1013 (s), 906 (w), 861 (w), 795 (vs), 703 (w). MS-FAB (NBA): *m*/*z* calcd for $C_{30}H_{54}BrNOP_2Ru$ = $[M - Br]^+$ 689.19, found 689.7. Elemental analysis (%) calcd for $C_{30}H_{54}Br_2NOP_2Ru$: C 46.94, H 7.09, N 1.82. Found: C 46.94, H 6.80, N 1.80.

[RuI$_{1-2}$(NO)(PCyp$_3$)$_2$]. Dipotassium pentaiodido nitrosyl ruthenate (0.898 g, 1.06 mmol), dissolved in ethanol–water (5 : 1, 30 mL), was added to a solution of tricyclopentylphosphane (1.00 g, 4.20 mmol) in hot ethanol (10 mL). The reaction mixture was kept under refluxing conditions for 45 minutes. The resulting dark green solid was collected by filtration and dried *in vacuo.* Yield: 1.02 g. ^{31}P NMR (109 MHz, C_7H_8, 25 °C) δ/ppm: 49.9, 34.2, 19.2, 16.8, 4.9. Selected IR bands ν_{max}/cm^{-1}: 2943 (w), 2864 (w), 2359 (w) 1750 (s), 1707 (s), 1446 (w), 1299 (w), 1260 (w), 1119 (w), 904 (w), 874 (w), 621 (vw). MS-FAB (NBA): *m*/*z* calcd for $C_{30}H_{54}INOP_2Ru$ = $[M - I]^+$ 735.18, found 735.4.

[RuCl$_{1-3}$(NO)(P^{i}Pr$_3$)$_2$]. Dipotassium pentachlorido nitrosyl ruthenate (1.48 g, 3.83 mmol), dissolved in ethanol–water (1 : 1, 60 mL), was added to a solution of triisopropylphosphane (1.50 g, 9.00 mmol) in hot ethanol (15 mL). The reaction mixture was kept under refluxing conditions for 1 hour. The resulting solid was collected by filtration and dried *in vacuo.* Yield: 1.17 g, 2.23 mmol, 58.3%. ^{31}P NMR (109 MHz, C_7H_8, 25 °C) δ/ppm: 33.2, 29.6, 27.1. Selected IR bands ν_{max}/cm^{-1}: 2958 (w), 1841 (m), 1804 (s), 1707 (vs), 1455 (m), 1366 (w), 1240 (m), 1061 (m), 882 (m), 655 (vs). MS-FAB (NBA):

m/z calcd for $C_{18}H_{42}ClNOP_2Ru$ = $[M - Cl]^+$ 522.12, found 522.4. Elemental analysis (%) calcd for $C_{18}H_{42}Cl_2NOP_2Ru$: C 41.38, H 8.10, N 2.68. Found: C 41.45, H 8.29, N 2.61.

$[RuBr_{1-3}(NO)(P^iPr_3)_2]$. Dipotassium pentabromido nitrosyl ruthenate (2.95 g, 4.84 mmol), dissolved in ethanol–water (1 : 1, 70 mL), was added to a solution of tri-isopropylphosphane (2.00 g, 12.5 mmol) in hot ethanol (20 mL). The reaction mixture was kept under refluxing conditions for 30 minutes. The resulting green solid was collected by filtration and dried *in vacuo.* Yield: 2.30 g. ^{31}P NMR (109 MHz, C_7H_8, 25 °C) δ/ppm: 48.1. Selected IR bands ν_{max}/cm^{-1}: 2955 (w), 1756 (m), 1705 (m), 1455 (w), 1365 (w), 1240 (w), 1060 (w), 1028 (w), 930 (w), 883 (m), 655 (vs), 624 (w). MS-FAB (NBA): *m/z* calcd for $C_{18}H_{42}BrNOP_2Ru$ = $[M - Br]^+$ 533.09, found 533.3.

$[RuCl(NO)_2(PPh_3)_2]BF_4$ (1). **1** was prepared on the basis of a published procedure. $[RuCl_3(NO)(PPh_3)_2]$ (0.23 g, 0.30 mmol) and zinc-copper alloy (1.62 g) were suspended in toluene (20 mL) and heated under reflux for 4.5 h. The initially chartreuse suspension turned green during the course of the reaction. To remove excess alloy, the suspension was filtered. Afterwards a solution of $NOBF_4$ (0.053 g, 0.45 mmol) in toluene–ethanol (10 mL/1.3 mL) was added, whereupon a rapid colour change from emerald-green to red-orange took place. Crystals were formed on cooling to ambient temperature. The yield (0.059 g, 0.073 mmol, 24%) was further increased by storage at 4 °C. The solid was filtered off, washed with *n*-hexane (5 mL) and dried *in vacuo*. ^{31}P NMR (109 MHz, CH_2Cl_2, 25 °C) δ/ppm: 30.8. Selected IR bands ν_{max}/cm^{-1}: 1842 (m, NO), 1685 (m, NO), 1482 (w), 1435 (m), 1191 (vw), 1095 (m), 1058 (vs), 997 (m), 747 (s), 713 (m), 689 (vs). MS-FAB (NBA): *m/z* calcd 721.05 for $[RuCl(NO)_2(PPh_3)_2]^+$ = $[M]^+$, found 721.05; *m/z* calcd 691.05 for $[RuCl(NO)(PPh_3)_2]^+$ = $[M - NO]^+$, found 691.10. Elemental analysis (%) calcd for **2**: C 53.52, H 3.74, N 3.47. Found: C 52.95, H 3.74, N 3.40.

$[RuBr(NO)_2(PPh_3)_2]BF_4$ (2). $[RuBr_3(NO)(PPh_3)_2]$ (0.269 g, 0.300 mmol) and zinc-copper alloy (1.59 g) were suspended in toluene (25 mL) and heated under reflux for 3.5 h. The initially green suspension turned dark green. To remove excess alloy, the suspension was filtered. Afterwards a solution of $NOBF_4$ (0.056 g, 0.48 mmol) in toluene–ethanol (10 mL/1.3 mL) was added, whereupon a rapid colour change from dark green to dark red orange occurred. Red orange crystals in the shape of blocks formed overnight. After keeping the solution at 4 °C for several days, the product was filtered off and washed with *n*-hexane (6 mL). It was freed from all volatile components *in vacuo*. Yield: 140 mg, 0.164 mmol, 54.8%. ^{31}P NMR (109 MHz, CH_2Cl_2, 25 °C) δ/ppm: 27.3. Selected IR bands ν_{max}/cm^{-1}: 1824 (w, NO), 1765 (m, NO), 1480 (vw), 1435 (m), 1312 (w), 1187 (w), 1092 (m), 1050 (vs), 997 (m), 751 (m), 736 (m), 689 (s). MS-FAB (NBA): *m/z* calcd 765.00 for $[RuBr(NO)_2(PPh_3)_2]^+$ = $[M]^+$, found 765.1; *m/z* calcd 735.00 for $[RuBr(NO)(PPh_3)_2]^+$ = $[M - NO]^+$, found 735.1. Elemental analysis (%) calcd for **3**: C 50.73, H 3.55, N 3.29. Found: C 50.53, H 3.64, N 3.22.

$[RuCl(NO)_2(PPh_2Bn)_2]BF_4$ (3). $[RuCl_3(NO)(PPh_2Bn)_2]$ (0.24 g, 0.30 mmol) and zinc-copper alloy (1.4 g) were suspended in toluene (20 mL) and heated at 85 °C for 1.5 h. During the reaction the initially orange suspension turned into an emerald green solution. To remove excess alloy, the suspension was filtered under an inert gas atmosphere. After addition of the green ruthenium solution to a solution of $NOBF_4$ (47 mg, 0.40 mmol) in toluene–ethanol (15 mL/1.3 mL), a rapid colour change from green to red-orange occurred. Within a few days ruby red crystals were detected at the bottom of the flask, which were separated by filtration and washed with *n*-hexane. The solid was then freed from all volatile components *in vacuo* Yield: 87 mg, 0.10 mmol, 34%. ^{31}P NMR (109 MHz, CH_2Cl_2, 25 °C) δ/ppm: 42.9. Selected IR bands ν_{max}/cm^{-1}: 1799 (m, NO), 1771 (s, NO), 1583 (vw), 1484 (vw), 1455 (vw), 1436 (m), 1406 (vw), 1312 (vw), 1185 (vw), 1130 (vw), 1197 (m), 1046 (vs), 997 (m), 917 (vw), 829 (m), 774 (m), 740 (m), 700 (s), 688 (s). MS-FAB (NBA): *m/z* calcd 749.16 for $[RuCl(NO)_2(PPh_2Bn)_2]^+$ = $[M]^+$, found 749.1; *m/z* calcd 719.15 for $[RuCl(NO)(PPh_3)_2]^+$ = $[M - NO]^+$, found 719.1. Elemental analysis (%) calcd for **4**: C 54.60, H 4.10, N 3.35. Found: C 54.32, H 4.07, N 3.32.

$[RuBr(NO)_2(PPh_2Bn)_2]BF_4$ (4). $[RuBr_3(NO)(PPh_2Bn)_2]$ (0.28 g, 0.31 mmol) and zinc-copper alloy (1.5 g) were suspended in toluene (20 mL) and heated at 85 °C for 3 h. The initially orange suspension turned dark green. For removal of excess alloy the suspension was filtered under an inert atmosphere. A solution of $NOBF_4$ (0.040 g, 0.34 mmol) in toluene–ethanol (10 mL/1.3 mL) was added, whereupon a rapid colour change from dark green to dark red-orange occurred. Dark red crystals formed overnight. After keeping the solution at 4 °C for several days, the product was filtered off, washed with diethyl ether (5 mL) and dried *in vacuo*. Yield: 14 mg, 0.016 mmol, 5.3%. ^{31}P NMR (109 MHz, CH_2Cl_2, 25 °C) δ/ppm: 39.4. Selected IR bands ν_{max}/cm^{-1}: 1817 (m, NO), 1776 (s, NO), 1495 (w), 1455 (w), 1435 (m), 1406 (w), 1312 (w), 1097 (s), 1046 (vs), 997 (s), 917 (w), 830 (s), 775 (s), 741 (s), 701 (s). MS-FAB (NBA): *m/z* calcd 793.03 for $[RuBr(NO)_2(PPh_2Bn)_2]^+$ = $[M]^+$, found 793.0; *m/z* calcd 763.03 for $[RuBr(NO)(PPh_3)_2]^+$ = $[M - NO]^+$, found 763.0. Elemental analysis (%) calcd for **5**: C 51.84, H 3.89, N 3.18, Br 9.08. Found: C 51.68, H 3.90, N 3.19, Br 9.00.

$[RuCl(NO)_2(PCy_3)_2]BF_4$ (5). $[RuCl_{1-3}(NO)(PCy_3)_2]$ (0.33 g) and zinc-copper alloy (2.8 g) were suspended in toluene (57 mL) and heated at 85 °C for 4 hours. The initially orange suspension turned dark green. After cooling to 50 °C the suspension was filtered in order to remove excess alloy. To the resulting solution, first ethanol (1.3 mL) and then $NOBF_4$ (in small quantities) were added until the colour changed from dark green to red-orange. Overnight red-orange crystals were obtained. Yield: 80 mg, 0.095 mmol. ^{31}P NMR (109 MHz, CH_2Cl_2, 25 °C) δ/ppm: 53.1. Selected IR bands ν_{max}/cm^{-1}: 2928 (w), 2849 (w), 1789 (m, NO), 1704 (m, NO), 1445 (w), 1176 (vw), 1046 (s), 889 (vw), 851 (w), 732 (w), 636 (w), 620 (vw). MS-FAB (NBA): *m/z* calcd 758.34 for $[RuCl(NO)_2(PCy_3)_2]^+$ = $[M]^+$, found 758.0; *m/z* calcd 728.34 for $[RuCl(NO)(PCy_3)_2]^+$ = $[M - NO]^+$, found 728.0. Elemental analysis (%) calcd for **6**: C 51.22, H 7.88, N 3.32. Found: C 51.06, H 7.30, N 3.28.

$[RuBr(NO)_2(PCy_3)_2]BF_4$ (6). $[RuBr_{1-3}(NO)(PCy_3)_2]$ (0.556 g) and zinc-copper alloy (3.11 g) were suspended in toluene

(40 mL) and heated at 85 °C for 5 hours. The initially orange suspension turned dark green. After cooling to ambient temperature the suspension was filtered in order to remove excess alloy. First ethanol (1.3 mL) and then $NOBF_4$ (s) were added to the solution at 50 °C. Overnight an orange-red precipitate formed, which was filtered off and recrystallised in dichloromethane and *n*-hexane. Yield: 419 mg, 0.472 mmol. ^{31}P NMR (109 MHz, CH_2Cl_2, 25 °C) δ/ppm: 50.4. Selected IR bands ν_{max}/cm^{-1}: 2925 (w), 2851 (w), 1785 (m, NO), 1714 (m, NO), 1445 (w), 1270 (vw), 1177 (vw), 1047 (vs), 1003 (m), 889 (vw), 851 (w). MS-FAB (NBA): *m*/*z* calcd 803.2827 for $[RuBr(NO)_2(PCy_3)_2]^+$ = $[M]^+$, found 803.2830; *m*/*z* calcd 771.2852 for $[RuBr(NO)(PCy_3)_2]^+$ = $[M - NO]^+$, found 771.2813. Elemental analysis (%) calcd for **7**·CH_2Cl_2: C 45.65, H 7.04, N 2.88. Found: C 45.51, H 7.14, N 2.97.

$[RuI(NO)_2(PCy_3)_2]BF_4$ (7). $[RuI_{1-2}(NO)(PCy_3)_2]$ (0.11 g) and zinc-copper alloy (2.7 g) were suspended in toluene (17 mL) and heated at 85 °C for 5 hours. The initially orange suspension turned dark green. After cooling to ambient temperature the suspension was filtered in order to remove excess alloy. Ethanol (1.0 mL) was added to the solution at 40 °C. Solid nitrosyl tetrafluoroborate was added at the same temperature. Overnight reddish brown crystals separated, which were washed with diethyl ether and dried *in vacuo.* Yield: 97 mg, 0.10 mmol. ^{31}P NMR (109 MHz, CH_2Cl_2, 25 °C) δ/ppm: 45.8. Selected IR bands ν_{max}/cm^{-1}: 2928 (m), 2855 (w), 1788 (m, NO), 1751 (m, NO), 1445 (m), 1271 (vw), 1213 (vw), 1174(vs), 1118 (w), 1049 (m), 889 (w), 851 (w), 744 (w). MS-FAB (NBA): *m*/*z* calcd 849.27 for $[RuI(NO)_2(PCy_3)_2]^+$ = $[M]^+$, found 849.9; *m*/*z* calcd 819.27 for $[RuI(NO)(PCy_3)_2]^+$ = $[M - NO]^+$, found 819.9. Elemental analysis (%) calcd for **8**: C 46.21, H 7.11, N 2.99. Found: C 45.01, H 6.84, N 2.86.

$[RuCl(NO)_2(PCyp_3)_2]BF_4$ (8). $[RuCl_{1-3}(NO)(PCyp_3)_2]$ (0.504 g) and zinc-copper alloy (1.55 g) were suspended in toluene (54 mL) and heated at 85 °C for 5 hours. The initially orange suspension turned dark green. After cooling to 50 °C the suspension was filtered in order to remove excess alloy. To the resulting solution first ethanol (1.8 mL) and then $NOBF_4$ (in small quantities) were added until the colour changed from dark green to red-orange. Overnight orange crystals could be obtained, which were filtered off, washed with diethyl ether and dried *in vacuo* Yield: 112 mg, 0.147 mmol. ^{31}P NMR (109 MHz, CH_2Cl_2, 25 °C) δ/ppm: 48.2. Selected IR bands ν_{max}/cm^{-1}: 2954 (w), 2870 (w), 1805 (m, NO), 1681 (m, NO), 1449 (w), 1087 (m), 1044 (vs), 714 (m). MS-FAB (NBA): *m*/*z* calcd 673.2398 for $[RuCl(NO)_2(PCyp_3)_2]^+$ = $[M]^+$, found 673.2436; *m*/*z* calcd 643.2418 for $[RuCl(NO)(PCyp_3)_2]^+$ = $[M - NO]^+$, found 643.2435.

$[RuBr(NO)_2(PCyp_3)_2]BF_4$ (9). $[RuBr_{1-3}(NO)(PCyp_3)_2]$ (0.588 g) and zinc-copper alloy (1.30 g) were suspended in toluene (44 mL) and heated at 85 °C for 5 hours. The initially orange suspension turned dark green. After cooling to 40 °C the suspension was filtered in order to remove excess alloy. To the resulting solution first ethanol (1.3 mL) and then $NOBF_4$ (in small quantities) were added until the colour changed from dark green to red-orange. Overnight red-orange crystals were obtained which were washed with diethyl ether and dried *in vacuo*. Yield: 156 mg, 0.194 mmol, 25.3%. ^{31}P NMR (109 MHz, CH_2Cl_2, 25 °C) δ/ppm: 43.7. Selected IR bands ν_{max}/cm^{-1}: 2958 (w), 2867 (w), 1810 (w, NO), 1770 (m, NO), 1448 (vw), 1299 (vw), 1245 (vw), 1137 (vw), 1085 (m), 1045 (vs), 906 (w), 193 (w). MS-FAB (NBA): *m*/*z* calcd 719.9 for $[RuBr(NO)_2(PCyp_3)_2]^+$ = $[M]^+$, found 719.8; *m*/*z* calcd 689.19 for $[RuBr(NO)(PCyp_3)_2]^+$ = $[M - NO]^+$, found 689.9. Elemental analysis (%) calcd for **11**: C 44.79, H 6.77, N 3.48. Found: C 44.60, H 6.47, N 3.45.

$[RuI(NO)_2(PCyp_3)_2]BF_4$ (10). $[RuI_{1-3}(NO)(PCyp_3)_2]$ (1.1 g) and zinc-copper alloy (2.1 g) were suspended in toluene (38 mL) and heated at 85 °C for 4.5 hours. The initially orange suspension turned dark green. After cooling to 50 °C the suspension was filtered in order to remove excess alloy. To the resulting solution first ethanol (3.3 mL) and then $NOBF_4$ (in small quantities) were added until the colour changed from dark green to red-orange. During the course of several days few reddish brown crystals were obtained. Yield: 0.22 g, 0.26 mmol. ^{31}P NMR (109 MHz, CH_2Cl_2, 25 °C) δ/ppm: 34.2. Selected IR bands ν_{max}/cm^{-1}: 2947 (w), 2867 (w), 1809 (m, NO), 1772 (m, NO), 1448 (w), 1300 (vw), 1245 (w), 1138 (w), 1087 (m), 1046 (s), 907 (w), 764 (w), 633 (w), 618 (w). MS-FAB (NBA): *m*/*z* calcd 765.1757 for $[RuI(NO)_2(PCyp_3)_2]^+$ = $[M]^+$, found 765.1716; *m*/*z* calcd 735.1778 for $[RuI(NO)(PCyp_3)_2]^+$ = $[M - NO]^+$, found 735.1802. Elemental analysis (%) calcd for **12**: C 42.32, H 6.39, N 3.29. Found: C 42.15, H 6.35, N 3.33.

$[RuCl(NO)_2(P^iPr_3)_2]BF_4$ (11). $[RuCl_{1-3}(NO)(P^iPr_3)_2]$ (0.285 g) and zinc-copper alloy (2.30 g) were suspended in toluene (27.3 mL) and heated at 85 °C for 4 hours. The initially orange suspension turned dark green. After cooling to 50 °C the suspension was filtered in order to remove excess alloy. To the resulting solution first ethanol (2.5 mL) and then $NOBF_4$ (in small quantities) were added until the colour changed from dark green to orange. After several hours orange crystals were obtained. Yield: 129 mg, 0.214 mmol, 39.2%. ^{31}P NMR (109 MHz, CH_2Cl_2, 25 °C) δ/ppm: 61.7. Selected IR bands ν_{max}/cm^{-1}: 2974 (vw), 1808 (w, NO), 1682 (m, NO), 1459 (w), 1391 (vw), 1255 (w), 1091 (m), 1047 (vs), 1026 (vs), 883 (w), 795 (w), 652 (m). MS-FAB (NBA): *m*/*z* calcd 517.1455 for $[RuCl(NO)_2(P^iPr_3)_2]^+$ = $[M]^+$, found 517.1461; *m*/*z* calcd 487.1474 for $[RuCl(NO)(P^iPr_3)_2]^+$ = $[M - NO]^+$, found 487.1479.

$[RuBr(NO)_2(P^iPr_3)_2]BF_4$ (12). $[RuBr_{1-3}(NO)(P^iPr_3)_2]$ (0.685 g) and zinc-copper alloy (2.56 g) were suspended in toluene (55 mL) and heated at 85 °C for 4 hours. The initially orange suspension turned dark green. After cooling to 50 °C the suspension was filtered in order to remove excess alloy. To the resulting solution first ethanol (2.5 mL) and then $NOBF_4$ (in small quantities) were added until the colour changed from dark green to red-orange. Overnight orange-brown crystals could be obtained. Yield: 361 mg, 0.557 mmol. ^{31}P NMR (109 MHz, CH_2Cl_2, 25 °C) δ/ppm: 59.8, 41.9. Selected IR bands ν_{max}/cm^{-1} = 1797 (m, NO), 1744 (m, NO), 1689 (m, NO), 1461 (w), 1248 (w), 10 921 (m), 1048 (vs), 1027 (vs), 880 (m), 673 (m), 648 (w). MS-FAB (NBA): *m*/*z* calcd 563.0943 for $[RuBr(NO)_2(P^iPr_3)_2]^+$ = $[M]^+$, found 563.0953; *m*/*z* calcd 531.0968 for $[RuBr(NO)(P^iPr_3)_2]^+$ = $[M - NO]^+$, found 531.0965.

Notes and references

1 J. A. McCleverty, *Chem. Rev.*, 2004, **104**, 403–418.
2 J. H. Enemark and R. D. Feltham, *Coord. Chem. Rev.*, 1974, **13**, 339–406.
3 N. L. Fry and P. K. Mascharak, *Acc. Chem. Res.*, 2011, **44**, 289–298.
4 A. W. Carpenter and M. H. Schoenfisch, *Chem. Soc. Rev.*, 2012, **41**, 3742–3752.
5 P. Coppens, I. Novozhilova and A. Kovalevsky, *Chem. Rev.*, 2002, **102**, 861–884.
6 T. E. Bitterwolf, *Coord. Chem. Rev.*, 2006, **250**, 1196–1207.
7 D. Schaniel and T. Woike, *Phys. Chem. Chem. Phys.*, 2009, **11**, 4391–4395.
8 D. Schaniel, T. Woike, N.-R. Behrnd, J. Hauser, K. W. Krämer, T. Todorova and B. Delley, *Inorg. Chem.*, 2009, **48**, 11399–11406.
9 D. Schaniel, T. Woike, B. Delley, D. Biner, K. W. Kramer and H.-U. Güdel, *Phys. Chem. Chem. Phys.*, 2007, **9**, 5149–5157.
10 A. Zangl, P. Klüfers, D. Schaniel and T. Woike, *Dalton Trans.*, 2009, 1034–1045.
11 A. Zangl, P. Klüfers, D. Schaniel and T. Woike, *Inorg. Chem. Commun.*, 2009, **12**, 1064–1066.
12 H. Giglmeier, T. Kerscher, P. Klüfers, D. Schaniel and T. Woike, *Dalton Trans.*, 2009, 9113–9116.
13 A. F. Vanin, R. R. Borodulin, L. N. Kubrina, V. D. Mikoyan and D. S. Burbaev, *Biophysics*, 2013, **58**, 103–109.
14 A. Klein, Y. v. Mering, A. Uthe, K. Butsch, D. Schaniel, N. Mockus and T. Woike, *Polyhedron*, 2010, **29**, 2553–2559.
15 J. Mason, D. M. P. Mingos, D. Sherman and R. W. M. Wardle, *J. Chem. Soc., Chem. Commun.*, 1984, 1223–1225.
16 D. Michael, P. Mingos, D. Sherman and S. Bott, *Transition Met. Chem.*, 1987, **12**, 471–475.
17 C. G. Pierpont, D. G. Van Derveer, W. Durland and R. Eisenberg, *J. Am. Chem. Soc.*, 1970, **92**, 4760–4762.
18 C. G. Pierpont and R. Eisenberg, *Inorg. Chem.*, 1972, **11**, 1088–1094.
19 L. K. Bell, J. Mason, D. M. P. Mingos and D. G. Tew, *Inorg. Chem.*, 1983, **22**, 3497–3502.
20 D. M. Mingos, D. Sherman and I. Williams, *Transition Met. Chem.*, 1987, **12**, 493–496.
21 L. A. Watson, M. Pink and K. G. Caulton, *J. Mol. Catal. A: Chem.*, 2004, **224**, 51–59.
22 M. R. Crimmin, R. G. Bergman and F. D. Toste, *Angew. Chem., Int. Ed.*, 2011, **50**, 4484–4487.
23 S. Alvarez, P. Alemany, D. Casanova, J. Cirera, M. Llunell and D. Avnir, *Coord. Chem. Rev.*, 2005, **249**, 1693–1708.
24 N. G. Connelly, T. Damhus, R. M. Hartshorn and A. T. Hutton, *Nomenclature of inorganic chemistry: IUPAC recommendations 2005*, The Royal Society of Chemistry, Cambridge, 2005.
25 A. W. Addison, T. N. Rao, J. Reedijk, J. van Rijn and G. C. Verschoor, *J. Chem. Soc., Dalton Trans.*, 1984, 1349–1356.
26 A. R. Rossi and R. Hoffmann, *Inorg. Chem.*, 1975, **14**, 365–374.
27 M. H. B. Stiddard and R. E. Townsend, *J. Chem. Soc. D*, 1969, 1372–1372.
28 D. J. Hodgson, N. C. Payne, J. A. McGinnety, R. G. Pearson and J. A. Ibers, *J. Am. Chem. Soc.*, 1968, **90**, 4486–4488.
29 J. R. Durig, W. A. McAllister, J. N. Willis and E. E. Mercer, *Spectrochim. Acta*, 1966, **22**, 1091–1100.
30 M. J. Cleare and W. P. Griffith, *J. Chem. Soc. A*, 1967, 1144–1147.
31 F. Neese, *Wiley Interdiscip. Rev.: Computational Molecular Science*, 2012, **2**, 73–78.
32 J. Cirera, E. Ruiz and S. Alvarez, *Chem. – Eur. J.*, 2006, **12**, 3162–3167.